ARTICLES
PUBLISHED ONLINE: 19 FEBRUARY 2012 | DOI: 10.1038/NCHEM.1272
nature chemistry

Imparting functionality to a metal–organic framework material by controlled nanoparticle encapsulation

Guang Lu[1], Shaozhou Li[1], Zhen Guo[2], Omar K. Farha[3], Brad G. Hauser[3], Xiaoying Qi[1], Yi Wang[2], Xin Wang[2], Sanyang Han[4], Xiaogang Liu[4,5], Joseph S. DuChene[6], Hua Zhang[1], Qichun Zhang[1], Xiaodong Chen[1], Jan Ma[1], Say Chye Joachim Loo[1,7], Wei D. Wei[6], Yanhui Yang[2], Joseph T. Hupp[3]* and Fengwei Huo[1]*

Microporous metal–organic frameworks (MOFs) that display permanent porosity show great promise for a myriad of purposes. The potential applications of MOFs can be developed further and extended by encapsulating various functional species (for example, nanoparticles) within the frameworks. However, despite increasing numbers of reports of nanoparticle/MOF composites, simultaneously to control the size, composition, dispersed nature, spatial distribution and confinement of the incorporated nanoparticles within MOF matrices remains a significant challenge. Here, we report a controlled encapsulation strategy that enables surfactant-capped nanostructured objects of various sizes, shapes and compositions to be enshrouded by a zeolitic imidazolate framework (ZIF-8). The incorporated nanoparticles are well dispersed and fully confined within the ZIF-8 crystals. This strategy also allows the controlled incorporation of multiple nanoparticles within each ZIF-8 crystallite. The as-prepared nanoparticle/ZIF-8 composites exhibit active (catalytic, magnetic and optical) properties that derive from the nanoparticles as well as molecular sieving and orientation effects that originate from the framework material.

Metal–organic frameworks (MOFs)[1–3] are permanently microporous materials synthesized by assembling metal ions with organic ligands in appropriate solvents. MOFs have crystalline structures and typically are characterized by large internal surface areas, uniform but tunable cavities and tailorable chemistry. These characteristics make them very promising for a variety of applications, including gas storage[4,5], chemical separation[6], catalysis[7,8], sensing[9] and drug delivery[10]. By serving as unique host matrices for various functional species, MOFs also offer the opportunity to develop new types of composite materials that display enhanced (gas storage) or new (catalytic, optical and electrically conductive) behaviours[11–18] in comparison to the parent MOF counterparts.

In particular, the incorporation of nanoparticles in MOFs attracts much attention because of the benefits of novel chemical and physical properties exhibited by certain classes of nanoparticles[19–22]. Nanoparticle/MOF composites can be prepared either by using MOFs as templates to generate nanoparticles within their cavities[23–32] or by encapsulating presynthesized nanoparticles in MOFs[33–37]. In the former case, small and naked nanoparticles or clusters are generated and embedded in the cavities of MOFs. In the latter, however, usually presynthesized nanoparticles are stabilized with certain surfactants, capping agents or even ions, and the nanoparticle hydrodynamic radius is much larger than the cavity size of the MOF. The nanoparticles do not occupy the MOF cavities, but instead are surrounded by grown MOF materials.

Although there are many reports on nanoparticle/MOF composites and their applications (mainly focused on heterogeneous catalysis and gas storage), this emerging area is characterized by significant challenges[28], several of which we address here. First, for researchers to exploit fully the well-defined pore structures of MOFs (for example, molecule-size-selective catalysis or sensing) the incorporated nanoparticles need to be confined completely within the framework material. Thus far, this requirement has proved challenging to satisfy[31–33]. Second, the ability to control the size, shape and composition of the incorporated nanoparticles is highly desirable, as such control should enable the relevant properties of the particles to be tuned systematically. In this regard, encapsulation strategies seem attractive, but as yet are not well developed. Third, to preserve the properties of nanoparticles (especially optical and catalytic properties), it is often important that they remain separated so that nanoparticle agglomeration is minimized. Nevertheless, the agglomeration of nanoparticles is a commonly observed complication with existing encapsulation strategies[34–37]. Fourth, effective control over the spatial distribution of one or more types of nanoparticles within the MOF matrix is largely lacking with existing strategies for encapsulation.

Here, we report an encapsulation strategy that allows any of several types of nanoparticles to be incorporated fully within crystals of a readily synthesized zeolitic imidazolate framework material, ZIF-8, in a well-dispersed fashion (Fig. 1). This strategy involves

[1]School of Materials Science and Engineering, Nanyang Technological University, 50 Nanyang Avenue, Singapore 639798, Singapore, [2]School of Chemical and Biomedical Engineering, Nanyang Technological University, 62 Nanyang Drive, Singapore 637459, Singapore, [3]Department of Chemistry, Northwestern University, 2145 Sheridan Road, Evanston, Illinois 60208, USA, [4]Department of Chemistry, National University of Singapore, Singapore 117543, Singapore, [5]Institute of Materials Research and Engineering, 3 Research Link, Singapore 117602, Singapore, [6]Department of Chemistry and Center for Nanostructured Electronic Materials, University of Florida, Gainesville, Florida 32611, USA, [7]Solar Fuels Laboratory, Nanyang Technological University, Singapore 639798, Singapore. *e-mail: fwhuo@ntu.edu.sg; j-hupp@northwestern.edu

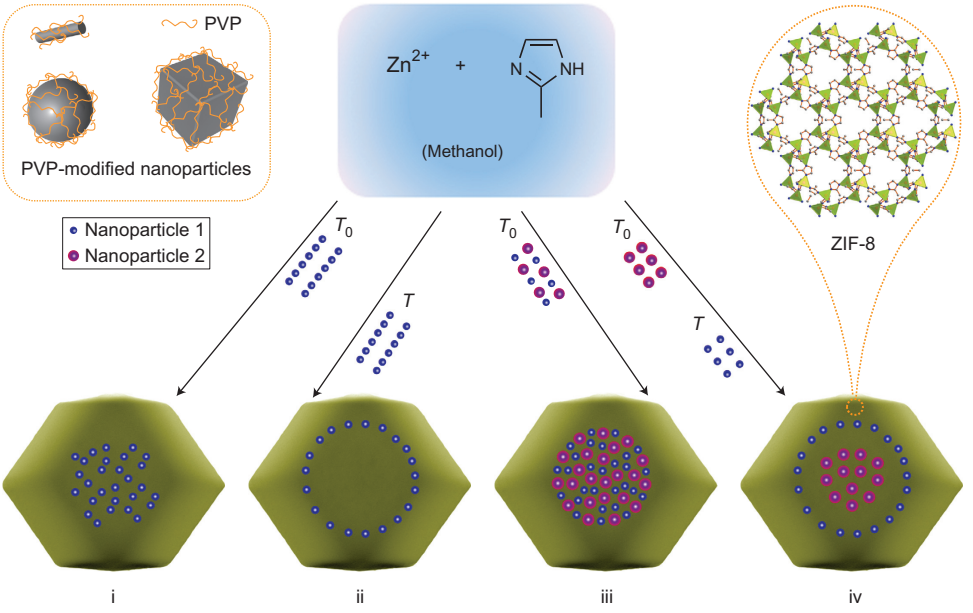

Figure 1 | Scheme of the controlled encapsulation of nanoparticles in ZIF-8 crystals. Through surface modification with surfactant PVP, nanoparticles of various sizes, shapes and compositions can be encapsulated in a well-dispersed fashion in ZIF-8 crystals, themselves formed by assembling zinc ions with imidazolate ligands. The spatial distribution of incorporated PVP-modified nanoparticles within ZIF-8 crystals can also be controlled by their addition sequence (that is, addition at the beginning (T_0) or after a certain time (T) during the MOF synthesis). Spatial distributions as a single type of nanoparticle in the central areas (i) or off the central areas (ii) of the MOF crystals, and as two types of nanoparticles in the central areas (iii) or one type in the central area but the other type in the transition layers (iv) of the MOF crystals.

the functionalization of nanoparticle surfaces with polyvinylpyrrolidone (PVP) and the optimization of the crystallization of ZIF-8. PVP is an amphiphilic, non-ionic polymer used extensively, not only as a 'general' surfactant to stabilize various nanoparticles in polar solvents (such as methanol and *N*,*N*-dimethylformamide, commonly used as solvents for MOF synthesis)[38], but also as a capping agent to assist in controlling the size and shape of certain nanoparticles during their syntheses[39]. ZIF-8, characterized by the sodalite zeolite-type structure and featuring large cavities (11.6 Å) and small apertures (3.4 Å), is well known for its chemical robustness and thermal stability[40]. ZIF-8 can be produced in the form of powders[40,41], thick membranes[42] and thin films[43] through diverse protocols. Nanoparticle/MOF composites were prepared by the crystallization of ZIF-8 in methanol at room temperature in the presence of PVP-modified nanoparticles under optimized experimental conditions.

In contrast to previous reports on nanoparticles used as seeds to induce the nucleation of MOF crystals[34–37], our strategy relies on the successive adsorption of nanoparticles onto the continuously forming surfaces of the growing MOF crystals. This allows ready control over the spatial distribution of nanoparticles within ZIF-8 crystals by adjusting the time of nanoparticle addition during the MOF-formation reaction. The as-prepared hybrid materials exhibit active (catalytic, magnetic and optical) properties that derive from the incorporated nanoparticles as well as size- and alignment-selective behaviour (namely, molecular sieving and regioselective guest reactivity) that originates from the well-defined microporous nature of the MOF component.

Results and discussion

Nanoparticles were synthesized using established methods and their surfaces were functionalized with PVP either during or after synthesis (Supplementary Fig. S1). The encapsulation procedure was demonstrated initially with 13 nm Au nanoparticles. In a typical experiment, methanolic solutions of zinc nitrate (25 mM, 5 ml), 2-methylimidazole (25 mM, 5 ml) and Au nanoparticles (1 ml) were mixed briefly and then kept at room temperature for 24 hours without stirring. At room temperature the position of the localized surface plasmon resonance (LSPR) band of the PVP-modified Au nanoparticles in methanol did not change if only zinc nitrate or 2-methylimidazole was introduced, which indicates that the dielectric constant, and therefore the chemical composition, of the local environment of the nanoparticles was not changed by introducing components in isolation (Supplementary Fig. S2). The pink solid obtained by combining the Au particles and ZIF-8 building blocks was collected by centrifugation and washed several times with methanol. The supernatant was transparent and colourless, and its ultraviolet–visible (UV-vis) absorption spectrum showed no detectable LSPR band (Supplementary Fig. S2), which implies that, after 24 hours of reaction, essentially all of the nanoparticles were incorporated in the composite product. Scanning electron microscopy measurements showed that the product consisted of isolated ~1.1 μm wide crystals of rhombic dodecahedral shape (~74%) together with intergrown crystals (~26%) (Supplementary Fig. S2). Transmission electron microscopy (TEM) images revealed that each crystal contained multiple Au nanoparticles that were fully MOF-encapsulated, yet well dispersed (Supplementary Fig. S2). Almost no unencapsulated particles were observed.

The encapsulation process was investigated further by time-dependent TEM analysis and UV-vis absorption measurements. Figure 2a is a TEM image of the product, obtained after just six minutes of reaction, in the form of hybrid spheres that possess an average diameter of 320 nm. The spheres were composed of coordination polymer as well as embedded and adsorbed Au nanoparticles. In addition, a few free Au nanoparticles were observed. After 30 minutes, the hybrid spheres grew larger (~730 nm) and exhibited configurations that comprised nanoparticle-rich cores and nanoparticle-free shells because of the depletion of free Au nanoparticles during the reaction (Fig. 2b). The hybrid spheres evolved to rhombic dodecahedral crystals after three hours (Fig. 2c). UV-vis absorption spectra of the reaction solution recorded during the several minutes of coordination-polymer formation revealed that

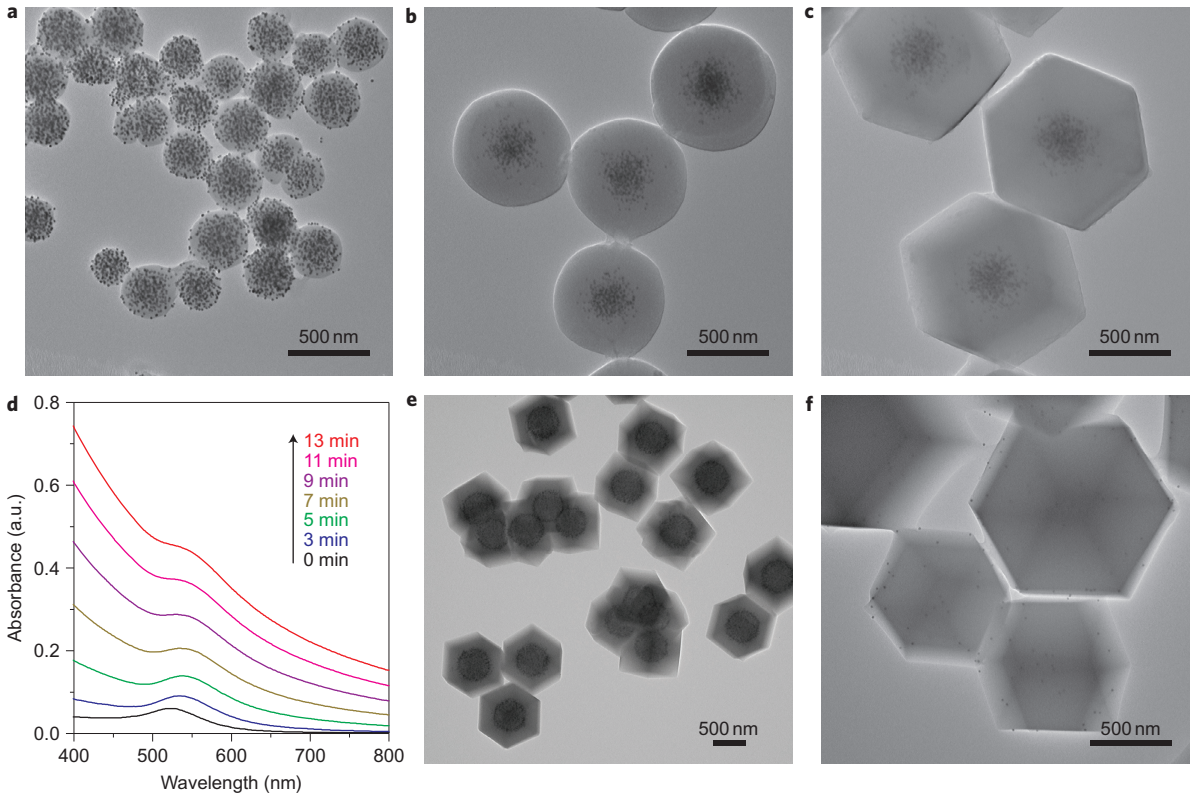

Figure 2 | TEM analysis and UV-vis absorption spectroscopy measurements of the encapsulation of 13 nm Au nanoparticles in ZIF-8 crystals. a–c, TEM images of the intermediate products of Au nanoparticle/ZIF-8 hybrid crystals collected after six minutes (**a**), 30 minutes (**b**) and three hours (**c**) of reaction. **d**, UV-vis absorption spectra of the reaction solution recorded in the initial 13 minutes. **e**, TEM image of hybrid crystals obtained when Au nanoparticles were introduced 15 minutes after the initiation of the reaction. **f**, TEM image of product obtained when excess free PVP was present in the reaction. a.u. = arbitrary units.

the LSPR band of the Au nanoparticles red-shifted rapidly from 520 nm to 540 nm (within five minutes) and simultaneously increased in intensity (Fig. 2d). Consistent with the TEM results, the former change reflects the occurrence of encapsulation that alters the dielectric constant of the local environment of the Au nanoparticles, whereas the latter reflects the growth of hybrid spheres that scatter light in the UV-vis range because of their large particle sizes[44]. More importantly, the essential absence of absorption peaks at longer wavelengths suggests that Au nanoparticles were well isolated from each other before and during the encapsulation process[45].

Under the crystallization conditions used, fast homogeneous nucleation of ZIF-8 (reaction solution in the absence of nanoparticles becomes turbid within five minutes) does not favour heterogeneous nucleation around nanoparticles or, at least, nanoparticle-induced nucleation is not dominant in the encapsulation process, which was supported further by follow-up experiments. We found that the encapsulation strategy still succeeded if nanoparticles were introduced at a certain time after initiation of the reaction instead of at the beginning. In this case, coordination-polymer spheres were formed through the homogeneous nucleation mechanism before the introduction of nanoparticles (Supplementary Fig. S4). The resuming reaction in the presence of nanoparticles produced hybrid crystals that consisted of the nanoparticle-free cores, nanoparticle-rich transition layers and nanoparticle-free shells (Fig. 2e). This result suggests that the encapsulation process does not rely on the heterogeneous nucleation mechanism, but instead is based on the succesive adsorption of PVP-modified nanoparticles on the continuously forming fresh surfaces of the growing coordination-polymer spheres until the particles are depleted. The adsorption of amphiphilic PVP on solid surfaces from a solution has been investigated extensively, and both the polar group (pyrrolidone ring) and apolar groups in the PVP structure are believed to contribute to the adsorption[46]. We therefore speculate that PVP adsorbed on nanoparticle surfaces not only stabilizes the nanoparticles in the reaction solution, but also provides the nanoparticles with an enhanced affinity to coordination-polymer spheres through weak coordination interactions between pyrrolidone rings (C=O) and zinc atoms in ZIF nodes, and perhaps also through hydrophobic interactions between apolar groups of PVP and organic linkers. To confirm this, excess free PVP was added intentionally in a control experiment. In the obtained product, we observed that only a few nanoparticles were adsorbed on the outer surfaces of the resulting crystals (Fig. 2f) and most nanoparticles remained in the reaction solution (Supplementary Fig. S5). This failed attempt to encapsulate nanoparticles suggests that the interaction between the PVP-modified nanoparticles and coordination-polymer spheres can be inhibited by the competitive adsorption of free PVP.

We found that the composite assembly strategy could be extended to other nanostructured objects of different sizes, shapes and compositions. For example, hybrid crystals that contained Pt (2.5, 3.3 and 4.1 nm), CdTe (2.8 nm), Fe_3O_4 (8 nm) and lanthanide-doped $NaYF_4$ (24 nm) nanoparticles, and Ag cubes (160 nm), polystyrene (PS) spheres (180 nm), β-FeOOH (22 nm × 160 nm) rods and lanthanide-doped $NaYF_4$ (50 nm × 310 nm) rods were prepared successfully using this strategy (Fig. 3 and Supplementary Fig. S6). The concentration of nanoparticles initially introduced to the reaction was optimized to ensure confinement of the nanoparticles exclusively within the crystals, after which the concentrations could be modulated to control the final content of nanoparticles in the hybrid crystals (Fig. 3a,b). We found that

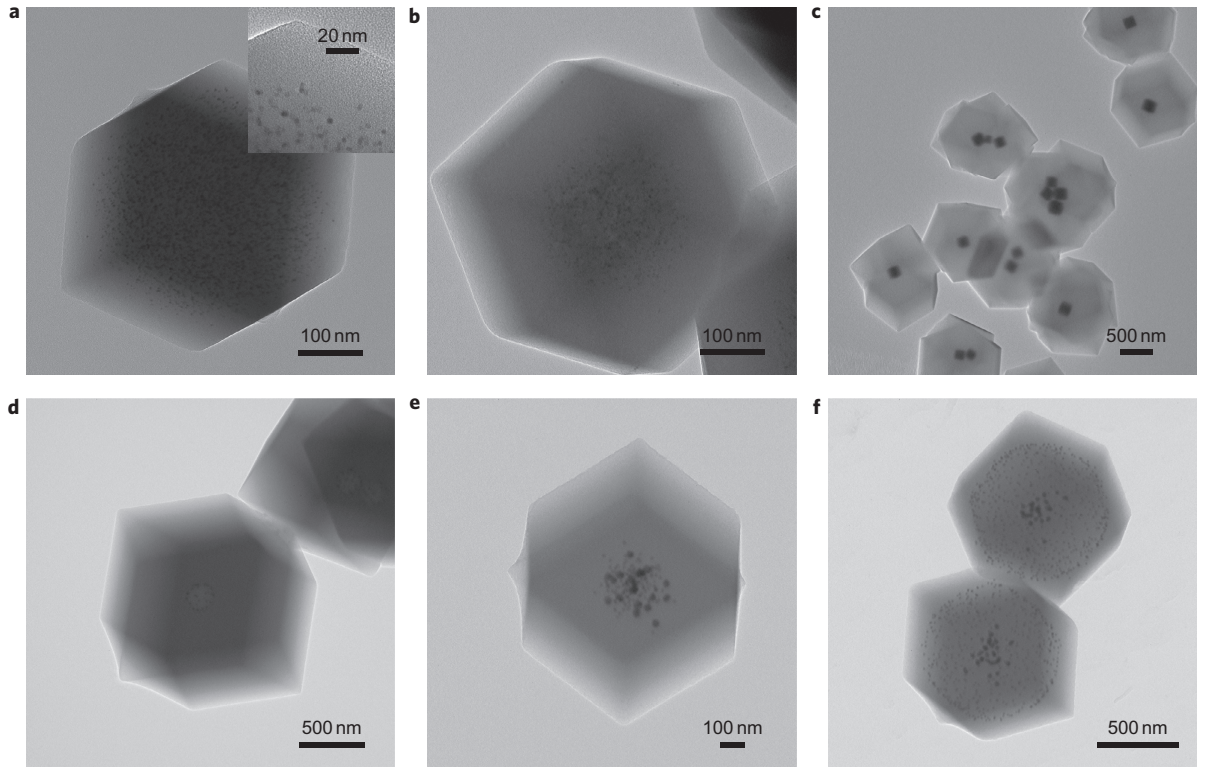

Figure 3 | TEM images of nanoparticle/ZIF-8 composites that contain different types of nanoparticles. a,**b**, Hybrid crystals that contain 3.3 nm Pt nanoparticles with Pt contents of 3.4% (**a**) (inset: high magnification image) and 0.7% (**b**), respectively. **c**, Hybrid crystals that contain Ag cubes (of average size 160 nm). **d**, Hybrid crystals that contain 180 nm PVP-modified PS spheres with surfaces that were partially coated with unmodified 13 nm Au nanoparticles. **e**, Hybrid crystal that contains homogeneously distributed 13 nm Au and 34 nm Au nanoparticles in the central area, prepared by simultaneously adding these two types of nanoparticles at the beginning of the reaction. **f**, Hybrid crystals that consist of 34 nm Au nanoparticle-rich cores, 13 nm Au nanoparticle-rich transition layers and nanoparticle-free shells prepared by sequentially adding 34 nm Au nanoparticles at the beginning of the reaction and 13 nm Au nanoparticles after 40 minutes.

nanoparticles with surfactant-free surfaces (a property important for catalysis applications) could also be introduced into the crystal matrix through their adsorption on the PVP-modified nanoparticles. For example, Fig. 3d shows a TEM image of the hybrid crystals that contain PVP-modified PS spheres with surfaces that were, in turn, partially coated with unmodified Au nanoparticles. The simultaneous encapsulation of different types of nanoparticles is possible with this strategy. Furthermore, their spatial distribution within MOF crystals can be controlled by the sequence of their addition during the assembly of the MOF. Taking advantage of this flexibility, we can disperse homogeneously two types of nanoparticles in the central areas of ZIF-8 crystals (Fig. 3e), or produce hybrid crystals that contain cores rich in one type of nanoparticles and transition layers rich in another type of nanoparticles (Fig. 3f and Supplementary Fig. S8).

As revealed by powder X-ray diffraction (XRD) measurements (Supplementary Fig. S9), all the hybrid materials exhibited diffraction patterns identical to that of ZIF-8. Compared to strong peaks that originate from ZIF-8 in diffraction patterns, peaks associated with nanoparticles within the crystals were too weak to be observed clearly, presumably because of their low concentrations and/or small sizes. However, their existence was confirmed by energy-dispersive X-ray microanalysis (Supplementary Fig. S10) and inductively coupled plasma analysis. Thermogravimetric analyses (Supplementary Fig. S12) indicate that nanoparticle/ZIF-8 composites are less thermally stable than pure ZIF-8, perhaps because of PVP-chain movement and decomposition (PVP glass transition temperature, 175 °C; decomposition temperature, 435 °C).

The permanent porosity of evacuated nanoparticle/ZIF-8 composites was confirmed by nitrogen-sorption measurements. The composites display type I isotherms, with steep increases in N_2 uptake at a low relative pressure (<0.01), as does ZIF-8, which indicates microporosity (Fig. 4a). Compared with pure ZIF-8, the composites show slightly decreased, gravimetric Brunauer–Emmett–Teller (BET) surface areas, as expected because of the contributions of non-porous Pt nanoparticles and PVP to the masses of the composites (Supplementary Table S1). However, the incorporation of nanoparticles does not alter the pore-size distribution of the MOF matrix, consistent with the fact that the introduced nanoparticles are too large to occupy the cavities (11.6 Å) of the framework (Fig. 4b).

The accessibility of embedded Pt nanoparticles modified with PVP for catalysis was first examined in CO oxidation. As shown in Supplementary Fig. S15, the Pt/PVP/ZIF-8 composite begins to catalyse oxidation of CO at 130 °C and conversion of nearly 100% is achieved at 200 °C. Combination of the catalysis properties of Pt nanoparticles and the molecular sieving capability of the ZIF-8 matrix was probed by examining the liquid-phase hydrogenation of *n*-hexene versus *cis*-cyclooctene. As shown in Fig. 5a, Pt/PVP/ZIF-8 does catalyse the hydrogenation of the linear *n*-hexene molecule (albeit with a low conversion, presumably because of slow diffusion through the small pore apertures (3.4 Å) of ZIF-8). The reusability of Pt/PVP/ZIF-8 as a catalyst for the hydrogenation of *n*-hexene was demonstrated by the observation of similar conversion efficiencies for consecutive runs (7.3%, 9.6% and 7.1% for the first, second and third runs, respectively). The mesoscopic structure of the catalyst/MOF hybrid material was preserved during the catalytic reactions and no degradation was detectable by TEM, XRD and Fourier transform infrared spectroscopy measurements (Supplementary Fig. S16). In contrast, the composite showed no

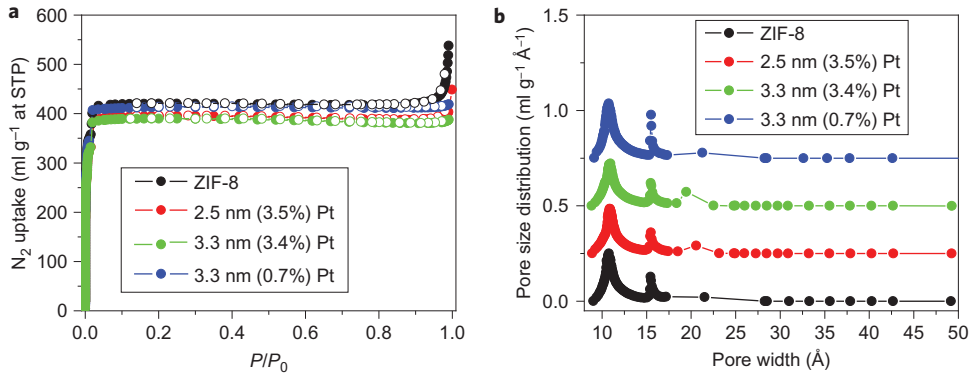

Figure 4 | Gas-sorption data for ZIF-8 and nanoparticle/ZIF-8 composites. a, Nitrogen-sorption isotherms for ZIF-8 and nanoparticle/ZIF-8 composites that contain 3.5% (2.5 nm), 3.4% (3.3 nm) and 0.7% (3.3 nm) Pt nanoparticles at 77 K up to 1 bar, which suggest slightly decreased gravimetric BET surface areas for nanoparticle/ZIF-8 composites. The solid and open symbols represent adsorption and desorption, respectively. **b**, Corresponding pore-size distributions calculated by the Horvath–Kawazoe method, which indicate that the incorporation of nanoparticles does not alter the pore-size distribution of the MOF matrix. The original curves for 2.5 nm (3.5%) Pt, 3.3 nm (3.4%) Pt, and 3.3 nm (0.7%) Pt samples have been shifted up by 0.25, 0.5, and 0.75 ml g^{-1} Å^{-1}, respectively, for clarity.

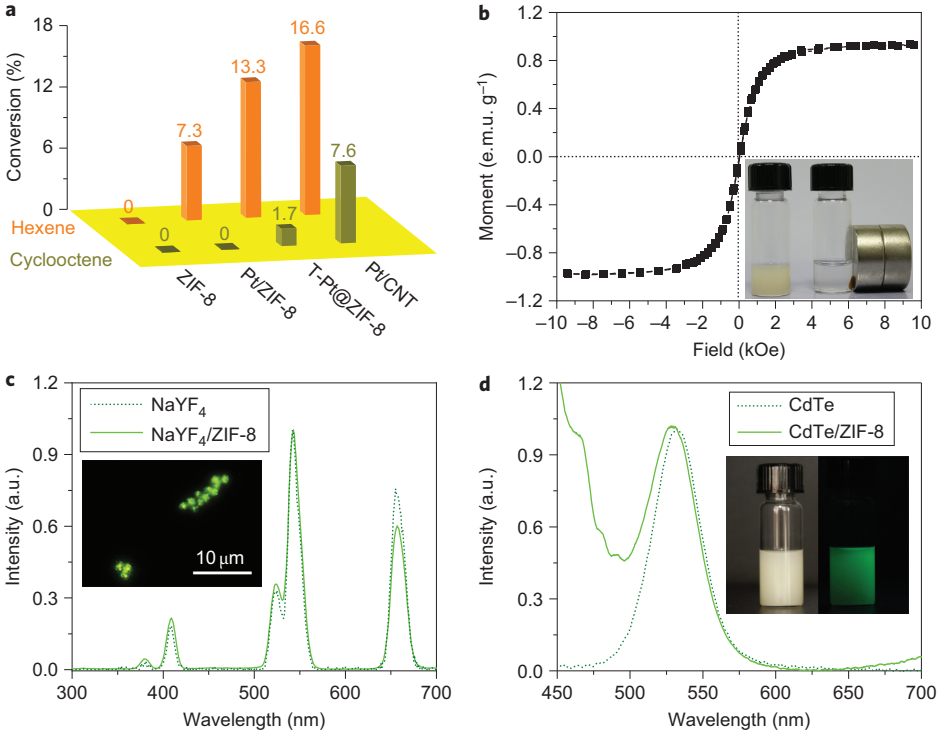

Figure 5 | Catalytic, magnetic and photoluminescence properties of nanoparticle/ZIF-8 composites. a, Size-selective hydrogenation of *n*-hexene and *cis*-cyclooctene catalysed by Pt/ZIF-8 composite (3.3 nm Pt nanoparticles, Pt content 2%). Pure ZIF-8, T-Pt@ZIF-8 composite (Pt content 2%) and Pt/CNT (Pt content 5%) were used as controls. **b**, Field-dependent magnetization curve of 8 nm Fe_3O_4/ZIF-8 composite at room temperature (inset: photograph of the collection of the composite by applying a magnetic field (right) to its suspension (left)). **c**, Normalized photoluminescence spectra with excitation at 980 nm for lanthanide-doped $NaYF_4$ rods (50 nm × 310 nm) (dotted line) and the corresponding $NaYF_4$/ZIF-8 composite (solid line) in methanol (inset: photoluminescence microscope image of the $NaYF_4$/ZIF-8 hybrid crystals excited at 980 nm). **d**, Normalized photoluminescence spectra with excitation at 400 nm for CdTe nanoparticles and the corresponding CdTe/ZIF-8 composite in methanol (inset: photographs of the CdTe/ZIF-8 composite suspended in methanol illuminated with ambient light (left) and 354 nm ultraviolet light (right)).

propensity to catalyse hydrogenation of the sterically more demanding cyclooctene, which is consistent with the small portal size for ZIF-8 (3.4 Å) and also suggests the substantial absence of Pt nanoparticles on the outer surface of the composite. In control experiments, pure ZIF-8 crystals showed no catalytic activity towards alkenes, but pure Pt nanoparticles (supported on carbon nanotubes (Pt/CNTs)) displayed indiscriminate catalysis of alkene hydrogenation. In contrast to the hybrid materials examined here, Pt/ZIF-8 composites prepared by a templating method (T-Pt@ZIF-8) showed selectivity for catalytic hydrogenation of *n*-hexene versus *cis*-cyclooctene. The observed residual activity for *cis*-cyclooctene hydrogenation evidently results from the non-preferential formation of naked nanoparticles within the cavities of MOF particles and on their outer surfaces (Supplementary Fig. S14); such behaviour is observed commonly in extensively reported templating approaches[28].

An additional set of experiments that involved Pt/PVP/ZIF-8 focused on the comparative reactivity of *n*-hexene versus *trans*-2-hexene. In the absence of the ZIF-8 shell, nanoparticulate platinum indiscriminately catalysed hydrogenation of the two alkenes. Once enshrouded, however, the catalyst partially hydrogenated the *n*-hexene sample (see above; experiments were not run to completion), but was completely inactive towards *trans*-2-hexene. Thus, the composite catalyst displayed, within experimental uncertainty, absolute regioselectivity and only hydrogenated terminal alkenes. To our knowledge, such selectivity has not been demonstrated previously for any platinum-containing composite or for any catalytic MOF material.

The field-dependent magnetization curve of the Fe_3O_4/ZIF-8 composite at room temperature is shown in Fig. 5b. The absence of hysteresis in the curve indicates the encapsulated oxides are superparamagnetic. The Fe_3O_4/ZIF-8 composite can be collected readily from a solvent suspension by applying a magnetic field. The remaining supernatant is transparent, which again indicates the high encapsulation efficiency of this strategy. Imparting photoluminescence properties to ZIF-8 particles was demonstrated by the separate encapsulation of each of two luminescent materials: lanthanide-doped $NaYF_4$ rods[47,48] and CdTe quantum dots[49]. As shown in Fig. 5c,d, both composites emit green light. In the case of $NaYF_4$/ZIF-8, the emission arises from upconversion of near-infrared radiation, and for CdTe/ZIF-8 the emission is a consequence of absorption of ultraviolet photons. The emission wavelength of the $NaYF_4$/ZIF-8 composite is identical to that of non-encapsulated rods in methanol, and that for CdTe/ZIF-8 is shifted slightly (from 532 nm to 529 nm) to that for free CdTe nanoparticles; this is consistent with the known slight sensitivity of the photoluminescence energies of these particles to the nature of their immediate environment[49]. To determine whether ZIF-8 can control molecular access to encapsulated semiconductor particles in much the same fashion as with catalytic Pt nanoparticles, we took advantage of the phenomenon of quenching of quantum-dot luminescence by molecular adsorbates[50]. Thus, we exposed samples of a CdSe/ZIF-8 composite to various thiol molecules (see Supplementary Fig. S18). We found that 2-mercaptoethanol can quench rapidly the emission of CdSe quantum dots encapsulated in ZIF-8 crystals, but that bulky cyclohexanethiol does not, which is consistent with efficient molecular sieving by ZIF-8 and with previous results that showed cyclohexane rings can be excluded by ZIF-8's small aperture[43].

Conclusions

In conclusion, we have demonstrated an effective strategy to encapsulate various nanoparticles within a readily assembled MOF material, ZIF-8, in a controllable way. This strategy is applicable to a broad range of nanoparticles, allows the incorporation of multiple nanoparticles in non-agglomerated fashion and is capable of controlling the spatial distribution of nanoparticles within the MOF matrix. The as-obtained nanoparticle/ZIF-8 composites encompass the benefit of porous and molecular sieving behaviour characterized by the MOF matrix, together with the functional behaviour characteristic of isolated nanoparticles.

Received 17 August 2011; accepted 17 January 2012; published online 19 February 2012

References

1. Férey, G. Hybrid porous solids: past, present, future. *Chem. Soc. Rev.* **37,** 191–214 (2008).
2. Yaghi, O. M. *et al.* Reticular synthesis and the design of new materials. *Nature* **423,** 705–714 (2003).
3. Horike, S., Shimomura, S. & Kitagawa, S. Soft porous crystals. *Nature Chem.* **1,** 695–704 (2009).
4. Rosi, N. L. *et al.* Hydrogen storage in microporous metal–organic frameworks. *Science* **300,** 1127–1129 (2003).
5. Murray, L. J., Dincă, M. & Long, J. R. Hydrogen storage in metal–organic frameworks. *Chem. Soc. Rev.* **38,** 1294–1314 (2009).
6. Li, J-R., Kuppler, R. J. & Zhou, H-C. Selective gas adsorption and separation in metal–organic frameworks. *Chem. Soc. Rev.* **38,** 1477–1504 (2009).
7. Lee, J. Y. *et al.* Metal–organic framework materials as catalysts. *Chem. Soc. Rev.* **38,** 1450–1459 (2009).
8. Ma, L., Abney, C. & Lin, W. Enantioselective catalysis with homochiral metal–organic frameworks. *Chem. Soc. Rev.* **38,** 1248–1256 (2009).
9. Allendorf, M. D., Bauer, C. A., Bhakta, R. K. & Houk, R. J. T. Luminescent metal–organic frameworks. *Chem. Soc. Rev.* **38,** 1330–1352 (2009).
10. Horcajada, P. *et al.* Porous metal–organic-framework nanoscale carriers as a potential platform for drug delivery and imaging. *Nature Mater.* **9,** 172–178 (2010).
11. Chae, H. K. *et al.* A route to high surface area, porosity and inclusion of large molecules in crystals. *Nature* **427,** 523–527 (2004).
12. Bureekaew, S. *et al.* One-dimensional imidazole aggregate in aluminium porous coordination polymers with high proton conductivity. *Nature Mater.* **8,** 831–836 (2009).
13. Hurd, J. A. *et al.* Anhydrous proton conduction at 150 °C in a crystalline metal–organic framework. *Nature Chem.* **1,** 705–710 (2009).
14. Lykourinou, V. *et al.* Immobilization of MP-11 into a mesoporous metal–organic framework, MP-11@mesoMOF: a new platform for enzymatic catalysis. *J. Am. Chem. Soc.* **133,** 10382–10385 (2011).
15. Larsen, R. W. *et al.* Mimicking heme enzymes in the solid state: metal–organic materials with selectively encapsulated heme. *J. Am. Chem. Soc.* **133,** 10356–10359 (2011).
16. Sun, C-Y. *et al.* Highly stable crystalline catalysts based on a microporous metal–organic framework and polyoxometalates. *J. Am. Chem. Soc.* **131,** 1883–1888 (2009).
17. Xiang, Z. *et al.* Metal–organic frameworks with incorporated carbon nanotubes: improving carbon dioxide and methane storage capacities by lithium doping. *Angew. Chem. Int. Ed.* **50,** 491–494 (2011).
18. Jahan, M., Bao, Q., Yang, J-X. & Loh, K. P. Structure-directing role of graphene in the synthesis of metal–organic framework nanowire. *J. Am. Chem. Soc.* **132,** 14487–14495 (2010).
19. Cushing, B. L., Kolesnichenko, V. L. & O'Connor, C. J. Recent advances in the liquid-phase syntheses of inorganic nanoparticles. *Chem. Rev.* **104,** 3893–3946 (2004).
20. Goesmann, H. & Feldmann, C. Nanoparticulate functional materials. *Angew. Chem. Int. Ed.* **49,** 1362–1395 (2010).
21. Shylesh, S., Schünemann, V. & Thiel, W. R. Magnetically separable nanocatalysts: bridges between homogeneous and heterogeneous catalysis. *Angew. Chem. Int. Ed.* **49,** 3428–3459 (2010).
22. Stark, W. J. Nanoparticles in biological systems. *Angew. Chem. Int. Ed.* **50,** 1242–1258 (2011).
23. Hermes, S. *et al.* Metal@MOF: loading of highly porous coordination polymers host lattices by metal organic chemical vapor deposition. *Angew. Chem. Int. Ed.* **44,** 6237–6241 (2005).
24. Houk, R. J. T. *et al.* Silver cluster formation, dynamics, and chemistry in metal–organic frameworks. *Nano Lett.* **9,** 3413–3418 (2009).
25. Zlotea, C. *et al.* Pd nanoparticles embedded into a metal–organic framework: synthesis, structural characteristics, and hydrogen sorption properties. *J. Am. Chem. Soc.* **132,** 2991–2997 (2010).
26. Jiang, H-L. *et al.* Au@ZIF-8: CO oxidation over gold nanoparticles deposited to metal–organic framework. *J. Am. Chem. Soc.* **131,** 11302–11303 (2009).
27. Esken, D. *et al.* Au@ZIFs: stabilization and encapsulation of cavity-size matching gold clusters inside functionalized zeolite imidazolate frameworks, ZIFs. *Chem. Mater.* **22,** 6393–6401 (2010).
28. Meilikhov, M. *et al.* Metals@MOFs-loading MOFs with metal nanoparticles for hybrid functions. *Eur. J. Inorg. Chem.* **2010,** 3701–3714 (2010).
29. Jiang, H-L. & Xu, Q. Porous metal–organic frameworks as platforms for functional applications. *Chem. Commun.* **47,** 3351–3370 (2011).
30. Gu, X., Lu, Z-H., Jiang, H-L., Akita, T. & Xu, Q. Synergistic catalysis of metal–organic framework-immobilized Au–Pd nanoparticles in dehydrogenation of formic acid for chemical hydrogen storage. *J. Am. Chem. Soc.* **133,** 11822–11825 (2011).
31. Park, T-H. *et al.* Highly dispersed palladium(II) in a defective metal–organic framework: application to C–H activation and functionalization. *J. Am. Chem. Soc.* **133,** 20138–20141 (2011).
32. Ameloot, R. *et al.* Metal–organic framework single crystals as photoactive matrices for the generation of metallic microstructures. *Adv. Mater.* **23,** 1788–1791 (2011).
33. Falcaro, P. *et al.* A new method to position and functionalize metal–organic framework crystals. *Nature Commun.* **2,** 237 doi: 10.1038/ncomms1234 (2011).
34. Lohe, M. R. *et al.* Heating and separation using nanomagnet-functionalized metal–organic frameworks. *Chem. Commun.* **47,** 3075–3077 (2011).
35. Buso, D., Nairn, K. M., Gimona, M., Hill, A. J. & Falcaro, P. Fast synthesis of MOF-5 microcrystals using sol–gel SiO_2 nanoparticles. *Chem. Mater.* **23,** 929–934 (2011).

36. Sugikawa, K., Furukawa Y. & Sada K. SERS-active metal–organic frameworks embedding gold nanorods. *Chem. Mater.* **23,** 3132–3134 (2011).
37. Tsuruoka, T., Kawasaki, H., Nawafune, H. & Akamatsu, K. Controlled self-assembly of metal–organic frameworks on metal nanoparticles for efficient synthesis of hybrid nanostructures. *ACS Appl. Mater. Interfaces* **3,** 3788–3791 (2011).
38. Li, Z. & Zhang, Y. Monodisperse silica-coated polyvinylpyrrolidone/$NaYF_4$ nanocrystals with multicolor upconversion fluorescence emission. *Angew. Chem. Int. Ed.* **45,** 7732–7735 (2006).
39. Sun, Y. & Xia, Y. Shape-controlled synthesis of gold and silver nanoparticles. *Science* **298,** 2176–2179 (2002).
40. Park, K. S. *et al.* Exceptional chemical and thermal stability of zeolitic imidazolate frameworks. *Proc. Natl Acad. Sci. USA* **103,** 10186–10191 (2006).
41. Cravillon, J. *et al.* Rapid room-temperature synthesis and characterization of nanocrystals of a prototypical zeolitic imidazolate framework. *Chem. Mater.* **21,** 1410–1412 (2009).
42. Bux, H. *et al.* Zeolitic imidazolate framework membrane with molecular sieving properties by microwave-assisted solvothermal synthesis. *J. Am. Chem. Soc.* **131,** 16000–16001 (2009).
43. Lu, G. & Hupp, J. T. Metal–organic frameworks as sensors: a ZIF-8 based Fabry–Pérot device as a selective sensor for chemical vapors and gases. *J. Am. Chem. Soc.* **132,** 7832–7833 (2010).
44. Liz-Marzán, L. M., Giersig, M. & Mulvaney, P. Synthesis of nanosized gold–silica core–shell particles. *Langmuir* **12,** 4329–4335 (1996).
45. Cho, E. C., Choi, S-W., Camargo, P. H. C. & Xia, Y. Thiol-induced assembly of Au nanoparticles into chainlike structures and their fixing by encapsulation in silica shells or gelatin microspheres. *Langmuir* **26,** 10005–10012 (2010).
46. Graf, C., Vossen, D. L. J., Imhof, A. & van Blaaderen, A. A general method to coat colloidal particles with silica. *Langmuir* **19,** 6693–6700 (2003).
47. Wang, F. *et al.* Simultaneous phase and size control of upconversion nanocrystals through lanthanide doping. *Nature* **463,** 1061–1065 (2010).
48. Wang, F. *et al.* Tuning upconversion through energy migration in core–shell nanoparticles. *Nature Mater.* **10,** 968–973 (2011).
49. Zhang, H. *et al.* From water-soluble CdTe nanocrystals to fluorescent nanocrystal–polymer transparent composites using polymerizable surfactants. *Adv. Mater.* **15,** 777–780 (2003).
50. Wuister, S. F., Donegá, C. D. M. & Meijerink, A. Influence of thiol capping on the exciton luminescence and decay kinetics of CdTe and CdSe quantum dots. *J. Phys. Chem. B* **108,** 17393–17397 (2004).

Acknowledgements

F.H. acknowledges financial support from Nanyang Technological University (start-up grant), the AcRF Tier 1 (RG 42/10) from the Ministry of Education, Singapore, and the Singapore National Research Foundation under the Campus for Research Excellence and Technological Enterprise programme Nanomaterials for Energy and Water Management. The Northwestern group acknowledges financial support from the Air Force Office of Scientific Research and Defense Threat Reduction Agency (grant no. HDTRA-09-1-0007). We thank J. Wang and L. You for the measurement of magnetization curves. We thank Y.M. Lam and J.Y. Lek for the gift of CdSe nanoparticles.

Author contributions

G.L. conceived the idea, designed and performed the experiments, analysed the results and co-drafted the manuscript. S.L. was primarily responsible for the TEM characterization. Z.G. and Y.Y. designed and performed the catalysis experiments. B.G.H., Y.W. and X.W. assisted with gas-sorption studies. X.Q. and H.Z. synthesized magnetic nanoparticles. S.H. and X.L. carried out the synthesis of upconversion nanocrystals and luminescence analysis of the corresponding composite materials. J.T.H. and O.K.F. contributed to the general methodology, assisted with data interpretation and reviewed the manuscript. F.H. supervised the project, helped design the experiments and co-drafted the manuscript. All authors contributed to the analysis of the manuscript.

Additional information

The authors declare no competing financial interests. Supplementary information accompanies this paper at www.nature.com/naturechemistry. Reprints and permission information is available online at http://www.nature.com/reprints. Correspondence and requests for materials should be addressed to J.T.H. and F.H.